Cross-Polarization Imaging and Micro-Raman Detection of Defects in the Epitaxy of 4H-SiC

O.J. GLEMBOCKI,[1,3] S.M. PROKES,[1] R.E STAHLBUSH,[1] and M.F. MACMILLAN[2]

1.—Naval Research Laboratory, Washington, DC 20375. 2.—Dow Corning Corporation, Midland, MI 48686. 3.—E-mail: glembocki@bloch.nrl.navy.mil

Cross-polarized imaging with an optical scanner and confocal μ-Raman spectroscopy have been used to reveal and to study structural defects in n-4H-SiC. We introduce a new method of polarized imaging that uses a combination of linear and circular polarization, which enhances contrast in images of defect regions. Regions that show intensity contrast have been observed to have characteristics of either low-angle grain boundaries or sharp lines of delineation between low and high strain areas. Different types of polytype inclusions have also been observed, and the material within the inclusions has been shown to be either 3C-SiC or 6H-SiC. Polytype inclusions occur as isolated features or form cores of holes, and they can form at any point of the growth.

Key words: Confocal micro-Raman, cross polarized imaging, 4H-SiC, structural defects, inclusions

INTRODUCTION

Silicon carbide is a material that is of significant technological and scientific interest because of its electronic and thermal properties. Both bulk and epitaxial SiC are critical to high-frequency radio-frequency electronics and to power electronics because of their thermal conductivity and large bandgap. In addition, because it is an indirect gap material, SiC should have long minority carrier lifetimes, which play an important role in power devices.[1–6]

However, SiC has many issues that must be resolved prior to insertion into real electronic systems. These include lower than expected minority carrier lifetimes (<1 μsec);[7,8] the formation of defects during bulk and epitaxial growth, and the formation and propagation of defects during device operation.[9,10]

The types of defects that are common in state-of-the-art SiC include point defects, polytype inclusions, micropipes, screw dislocations, low-angle grain boundaries, misoriented areas, basal-plane dislocations, and stacking faults. Some of the causes of these defects include nonuniform temperatures and particulate formation during growth and low activation energy barriers between the various polytypes of SiC.[6]

(Received August 23, 2004; accepted January 3, 2005)

To advance the growth of high quality SiC, it becomes important to detect and to identify the defects that are produced during the growth of SiC. In this paper, we have combined cross-polarized imaging with Raman spectroscopy to examine extended defects. Cross-polarized imaging, which is commonly used to reveal extended defects in SiC provides optical maps of regions of a wafer that contain defects.[11] The optical signatures of many of the observed defects are unique but are not well understood. In order to identify the optical features, a second technique that is sensitive to structural properties is required. Although there has been work using x-ray topography, this technique lacks depth resolution.[12,13] By contrast, confocal μ-Raman spectroscopy can have depth resolutions approaching several microns, and with μ-Raman spectroscopy it becomes possible to determine the nature of the features that are observed in cross-polarized imaging and to determine their depth below the SiC surface. This enables us to ascertain at which stage of the growth process these defects form.

BACKGROUND

Cross-Polarized Imaging

As noted earlier, cross-polarized imaging is commonly used to reveal defects in transparent materials. The method is implemented in the following manner.

The material of interest is placed between two polarizers whose polarization directions are perpendicular to the plane of propagation and at 90° to each other. In this cross-polarized configuration, an isotropic and defect-free material placed between the two polarizers appears black. On the other hand, if the material exhibits birefringence that lies in the plane of polarization or any structural anisotropy that leads to birefringence, then the incident polarization is rotated and the resulting image contains bright regions.

While this approach is very useful for qualitative detection of defects in materials such as SiC, it does not reveal the structural properties or the specific identity of the defect. For example, polytype inclusions, localized strain fields caused by dislocations, and low-angle grain boundaries all produce bright regions in a cross-polarized image. By examining a simple cross-polarized image one cannot easily distinguish between them. However, once the optical signature associated with a particular defect is known, cross-polarized imaging can be used as a wafer-scale optical characterization technique.

Micro-Raman Scattering

Raman spectroscopy is a powerful optical probe of vibrational properties of solids. From the spectral line positions and their relative intensities, it is possible to identify a material, to determine its crystallographic orientation, and to ascertain the presence of local strain. This technique has been widely used to study structural properties of various materials, including semiconductors, polymers, gases, and liquids. In confocal μ-Raman spectroscopy, a high magnification objective, typically 50× or 100× is used to focus the probe laser to a spot size of 1 μm or better. On the detection side of the apparatus, a small pinhole is used to limit the depth of focus of the detected scattering to 2–3 μm in the best cases. This allows both depth and spatial profiling of very small structures.[14]

EXPERIMENTAL DETAIL

Samples

The samples used in this work were epitaxial 4H-SiC samples grown by chemical vapor deposition on 2-in.-diameter, heavily doped 4H-SiC substrates. They had the same layer structure as used for PiN diodes. The layers were 2-μm-thick, 10^{18} cm^{-3} nitrogen-doped buffer, followed by a 100-μm-thick drift layer that had a doping density of 10^{14} cm^{-3}, and capped with a 2-μm-thick, p^+ SiC layer. The substrate was titled 8° away from the C plane along (1120) to facilitate step flow growth.

Cross-Polarized Imaging

The cross-polarized imaging was performed using an Epson Perfection 3200 optical scanner (Nagano, Japan) that was equipped with a transparency (negative) scanning capability. The optical resolution of the scanner was 6,400 dpi optical, which corresponds to a spatial resolution of 6 μm. In addition, the scanner has a depth of focus of 2–3 cm. This scanning mode, in which the transparency (or negative) is illuminated from above and the transmitted light is detected below is ideal for scanning transparent wafers and allows us to obtain optical transmission data across the entire wafer.

For cross-polarized imaging, the wafer was placed between two 90-mm-diameter linear polarizers. The sandwich was subsequently scanned in transparency mode, and the scanner software controlled the exposure for the scan.

We also used an optical configuration in which the top linear polarizer (closest to the light source) was replaced with a circular polarizer. In this mode, one observes not only birefringent defects, but one also observes the parallel, polarized light transmission through the wafer. This mode enhances the contrast produced by defects. In addition, because it also passes transmitted light, it has potential for revealing doping density variations through the light that is absorbed by 4H-SiC at 2.7 eV.

Micro-Raman Spectroscopy

The confocal μ-Raman system that was used consisted of a Mitutoyo Microscope (Aurora, IL) and a SPEX (Edison, NJ) Triplemate spectrometer equipped with a charge couple device (CCD). The 514.5-nm line of an Ar ion laser was used as the excitation source and the laser had a power of 25 mW or less. The microscope had 10×, 50×, and 100× objectives for focusing the laser light and was coupled to the spectrometer through a fiber optic bundle. The light from the microscope was filtered by a 514.5-nm notch filter and focused onto the fiber through confocal pinholes that had diameters of 250 μm and 100 μm. In this configuration, we achieved a lateral spatial resolution of 0.7 μm and a depth resolution of 15 μm. The positions of Raman lines in a given spectrum were calibrated against a 546.0-nm line emission from a fluorescent light source. This line was present in all of the Raman data that was obtained.

This microscope system is also equipped with polarizers and bottom illumination. The polarizers are located so that the illumination light source and detection optics can be independently polarized. This configuration allows us to perform cross-polarized imaging using the microscope and to readily locate features observed in the full wafer scans using the scanning method described previously. It is important to note that while cross-polarized imaging could be performed using the microscope, there are issues of non-normal light incidence that only allow locating local structure of interest for Raman spectroscopy. In addition, full wafer scanning and post-scan image stitching increases processing time.

The sample was placed on a glass plate that was part of a computer-controlled Prior stage having 4-in. travel with submicron resolution. In addition, the focus of the microscope was electronically controlled with a resolution of less than 1 μm. This

configuration allowed for accurate spatial and depth profiling.

We used the following procedure in our measurements. Full wafer scans were obtained using the optical scanner. Features of interest were identified from the images. The sample was transferred to the μ-Raman system and the features of interest were located by using the electronic stage and by viewing the wafer in cross-polarized mode. Raman data were obtained as a function of lateral and depth position.

RESULTS

Cross-Polarized Imaging

Shown in Fig. 1 is a cross-polarized image for one of the 4H-SiC wafers used in this study. This image was obtained using the optical scanner. The area outside the wafer is black because of the low transmission through the crossed polarizers. The wafer appears bright and various extended defects are detected. On the periphery of the wafer, there are many larger areas containing polytype inclusions. Toward the center in the 5 o'clock position, there are many smaller circular and darker features, which are pits. In addition, the image shows many smaller structures characterized by intensity variations. These can be caused by a variety of defects that rotate the polarization. Some of the candidate defects are low-angle grain boundaries, strain fields caused by micropipes, micropipe groups, and clusters of dislocations.

The slight overall decrease in brightness toward the top of the wafer is caused by the 8° off-axis tilt of the substrate. The index of single-crystal SiC differs along the C axis and perpendicular to it. This birefringence leads to a displacement of the ordinary and extraordinary components of light passing through the wafer and results in the intensity banding observed in the image.

While the image in Fig. 1 exhibits numerous contrast features, it lacks information about doping densities. In addition, the contrast in many features near the center of the wafer is not very strong. An alternate approach that improves the quality of the image is to replace the incident light (top) linear polarizer with a circular polarizer. This configuration has two advantages over the first. The circularly polarized light allows the observation of normal transmission through the sample and enhances the contrast observed in the cross-polarized images.

Shown in Fig. 2 is an image taken for the same wafer as in Fig. 1. The first thing to note is that the region around the wafer is no longer black. This is a result of the fact that the combined circular and linear polarizers pass 50% of the incident light. The wafer has an overall green coloration that is not shown here and the presence of a darker (green) spot in the center of the wafer. The green color is caused by the heavy n-type doping level of 10^{18} cm^{-3}. At this doping density, there is significant intra-conduction band absorption at 2.7 eV, giving the wafer its green color. The darker spot in the middle is caused by a higher doping density and is common in n^+ 4H-SiC.

In addition, the contrast caused by defects is much better in Fig. 2 compared to Fig. 1. The contrast is improved because the direction of the defect-induced birefringence is not the same for all of the defects. Under illumination with linearly polarized light, defects that align with the polarization direction will

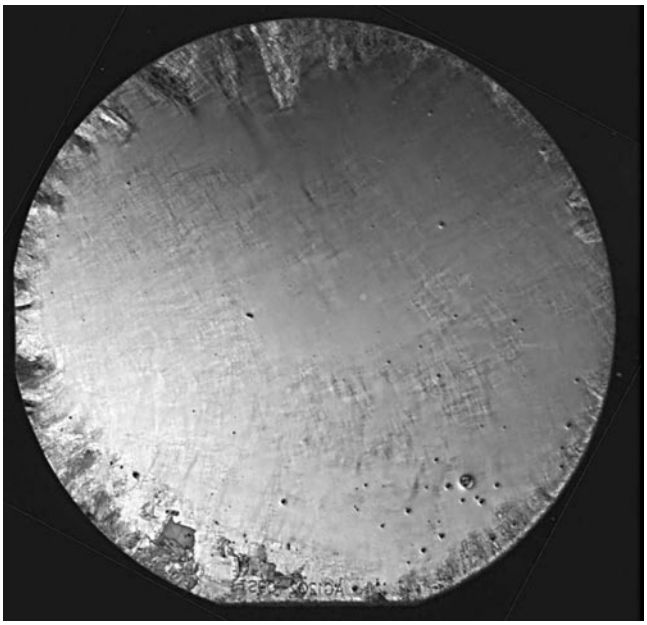

Fig. 1. The cross-polarized image of a 2-in.-diameter, 4H-SiC PIN diode wafer. The area outside the wafer is dark because of the crossed polarizers. The features at the periphery of the wafer are caused by polytype inclusions. There are also holes and finer contrast features away from the edges.

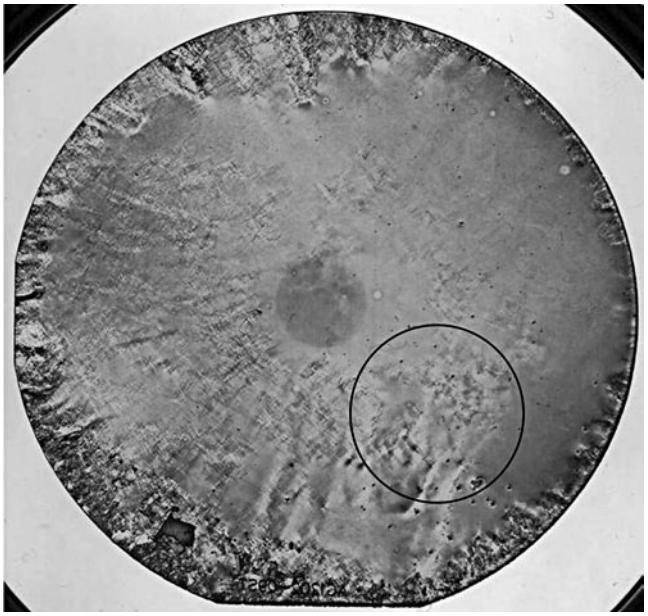

Fig. 2. The circular-linear polarized image of the same 2-in.-diameter, 4H-SiC PIN diode wafer shown in Fig. 1. The top polarizer (at the light source) is circular, while the analyzing polarizer (at the CCD detectors) is linear. Note that the area outside of the wafer is bright because this configuration does not extinguish all of the light. The circle indicates the region in which Raman analysis was performed.

display a contrast, whereas defects of any rotational orientation will create contrast when illuminated with circularly polarized light. This accounts for the increase in contrast and detail in the image of Fig. 2.

μ-Raman Spectroscopy

There are a significant number of features in the cross-polarized images of the wafer shown in Figs. 1 and 2. The physical causes for these features cannot be understood without the aide of a second probe that is sensitive to local structure. Because Raman spectroscopy is sensitive to structural properties through the vibrational modes of a semiconductor, it allows us to obtain more detail about features that are observed in the images in Figs. 1 and 2. Because a complete report of all of the features in the polarized light images is beyond the scope of this paper, we only consider three types of common defects: lines of cross-polarized contrast, holes, and regions separated by cracks. The circle in Fig. 2 outlines the region in which Raman spectroscopy was performed.

Contrast Variations in Cross-Polarized Images

The first type of defect that is common in cross-polarized images is an area of high and low contrast separated by a well-defined line. Figure 3 shows a picture of this type of defect taken in cross-polarized mode with the Raman microscope. This defect was located in a region of good quality SiC. The very small bright spot near the line is the laser spot used to obtain the Raman data. Raman spectra were taken on both sides of the line using spots separated by 3 μm. Below the image are Raman spectra for the two positions around the defect. A shift of peak positions of 0.6 cm^{-1} is observed between the two sampling locations. This indicates that there is more strain on the brighter side of the line. Through the use of phonon deformation potentials and the observed shifts in the phonon frequencies, we can estimate the strain within the bright region. However, deformation potentials are not available for 4H-SiC, so in our calculation, we use phonon deformation potentials for 3C-SiC.[15–17] By assuming a biaxial strain, we estimate a tensile strain of order 10^{-4} in $\Delta a/a$ in the bright region.

Furthermore, we note that the ratios of the intensities of the FTO(E_1) and FTO(E_2) phonon modes is different. In normal backscattering geometry, the FTO(E_1) mode is expected to be zero, while in right-angle scattering it will be strong.[18] Thus, the ratio of intensities of the two modes is a measure of the misalignment of the C plane relative to the normal to the sample. We note that the intensity of the FTO(E_1) relative to the FTO(E_2) mode is greater in the bright region than on the dark side. This indicates that in addition to strain, there is also lattice misalignment. It is also important to note that depth profiling showed similar spectra to that shown in Fig. 3, indicating that the strain fields extended for many tens of microns into the volume of the wafer.

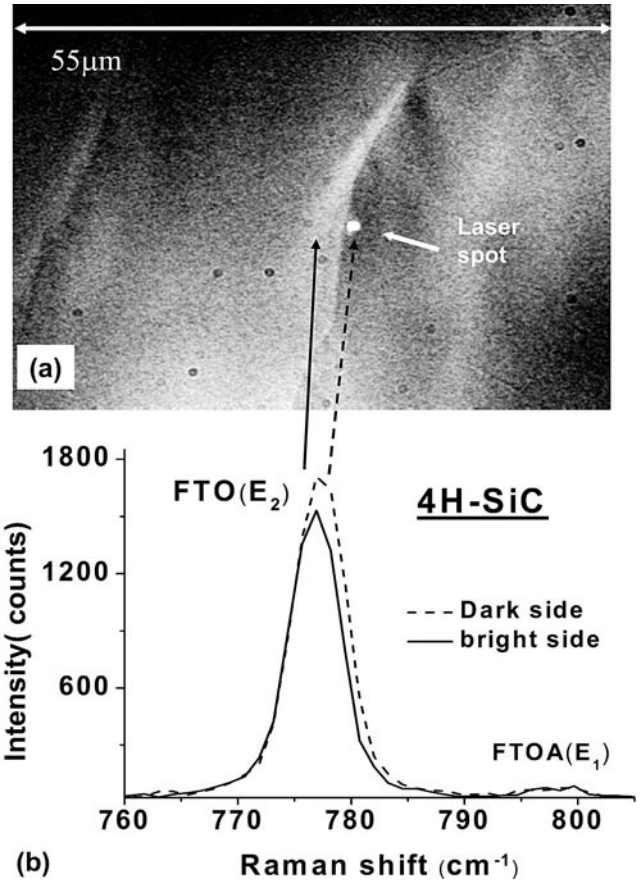

Fig. 3. (a) A cross-polarized microscope image of a contrast defect showing a sharp delineation between light and dark areas. (b) The Raman data from the dark and bright sides of the defect are shown below the image. The black arrows point to the location from which the data were obtained. The solid (dashed) designations for both the Raman data and the arrows correspond to the light (dark) side of the defect.

Another common type of contrast feature found in many cross-polarized images is shown in Fig. 4. This feature has no well-defined lines that delineate the bright and dark regions. Instead, the contrast variation is gradual and continuous. The Raman spectra from this type of defect are shown in Fig. 4b. In this case, the Raman lines from the two regions occur at the same position, indicating that there is no strain in the bright area. The relative intensities of the FTO(E_1) and FTO(E_2) phonon modes are different. As in the previous case, the bright region has a larger relative intensity of the FTO(E_1) phonon mode, indicating misorientations in the bright region. By comparing the ratio in the dark region to the ratio in the light region and knowing that the wafer has an 8° miscut, we can estimate the angle of the misorientation is approximately 1.5°.[18] The Raman data might suggest the presence of a low-angle grain boundary or a cluster of dislocations. Depth profiling of this region indicates that this feature is in the top 50 μm of the epitaxial layer.

Both of the defects discussed here show interesting properties that lead to birefringence and optical signatures in cross-polarized imaging. The Raman

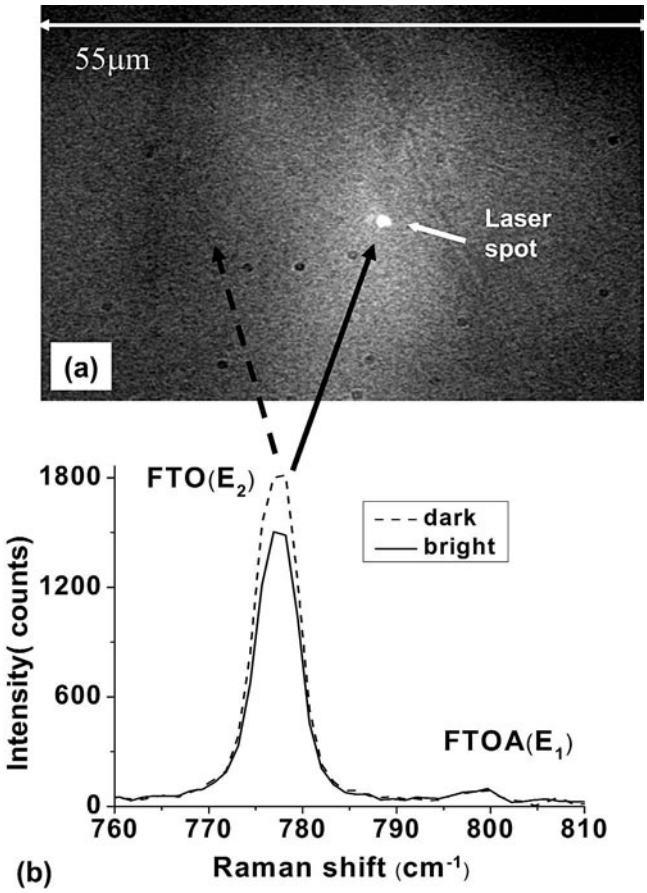

Fig. 4. A cross-polarized microscope image of a contrast defect showing a smoothly varying delineation between light and dark areas. The Raman data from the dark and bright sides of the defect are shown below the image. The arrows point to the regions from which the data were obtained.

spectroscopy studies show that strain and crystallographic misorientations are key players in the properties of these defects. However, more precise experiments using transmission electron microscopy are needed to identify the defects.

Inclusions

Other features that appear in cross-polarized images and often in unpolarized images are holes of various sizes and shapes and regions of different polytypes. While polytype inclusions are easy to observe in cross-polarized imaging, their crystalline structure and extent in depth are much harder to determine. Confocal Raman scattering can be used to resolve both issues. First, the various polytypes of SiC have distinct Raman spectra, facilitating identification. Furthermore, as shown in Fig. 5, the confocal nature of our Raman measurements allows us to probe a cylindrical volume of 15-μm depth and 0.7-μm diameter. With this, we can determine the physical extent of a defect.

In this paper, we will examine two types of holes and a polytype region. The first hole shown in Fig. 6a is quite large, approximately 80 μm in diameter, and has arrow-like features on one side of its outer

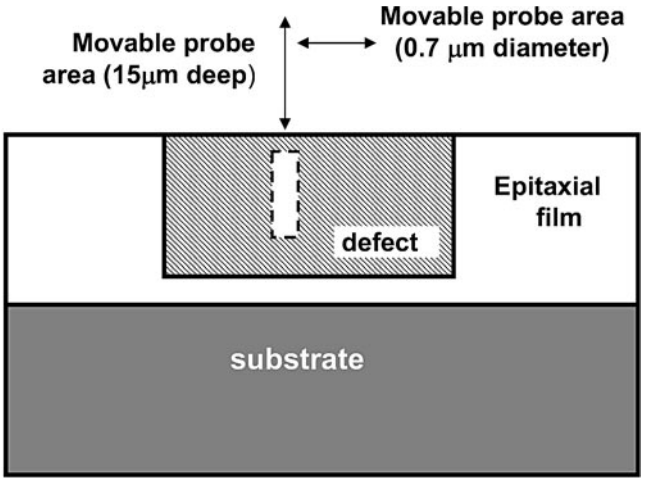

Fig. 5. Schematic representation of the volume probed by the confocal Raman system. The volume is a cylinder that has a diameter 0.7 μm and a depth of 15 μm. The side view of this cylinder is shown as a rectangle with dashed lines. The cylindrical volume can be scanned across the wafer in x, y, and z directions with 0.1-μm resolution.

periphery. A careful examination of the image by changing the focal point reveals a feature approximately 20 μm above the surface of the sample.

Raman spectra were collected to determine the nature of this defect. Shown in Fig. 6b are Raman spectra as a function of depth. The spectrum (solid line) taken from the surface of the inclusion, which is 20 μm above the surrounding areas, shows that it is pure crystalline 3C-SiC.[17] Moving the focus 100-μm inward places the focal point at the film/substrate interface. Here, the Raman data (dashed line) shows a presence of 4H-SiC, which tells us that the 3C-SiC within the hole began to grow at or near the substrate/epi interface. Probing around the periphery of the hole and its rim shows no strain. This indicates that the inclusion is separated from the walls of the hole.

This type of inclusion can occur if there was a defect present at the substrate at the spatial location of the hole. The fact that the 3C-SiC inclusion is 20 μm above the surface can be caused by either an increased growth rate of the 3C-SiC compared to the surrounding 4H-SiC or a Si particulate of approximately 20-μm diameter at the film/substrate interface.

The next type of inclusion that we studied is shown in Fig. 7a. The hole is pear shaped; the inclusion lies within the hole, and unlike the previous case, it is below the surface. The core of the hole is actually 5 μm below the surface. Figure 7b shows the Raman spectra taken in the inclusion and from areas surrounding it. The spectrum from the inclusion (solid line) shows lines from 4H-SiC and an additional line at 790 cm^{-1} that is characteristic of 6H-SiC.[17] Because the depth resolution for this measurement is 15 μm and because this line is much weaker than the 4H-SiC lines, we conclude that the inclusion is much less than 15 μm in thickness. Only 4H-SiC (dotted line) is observed when moving the

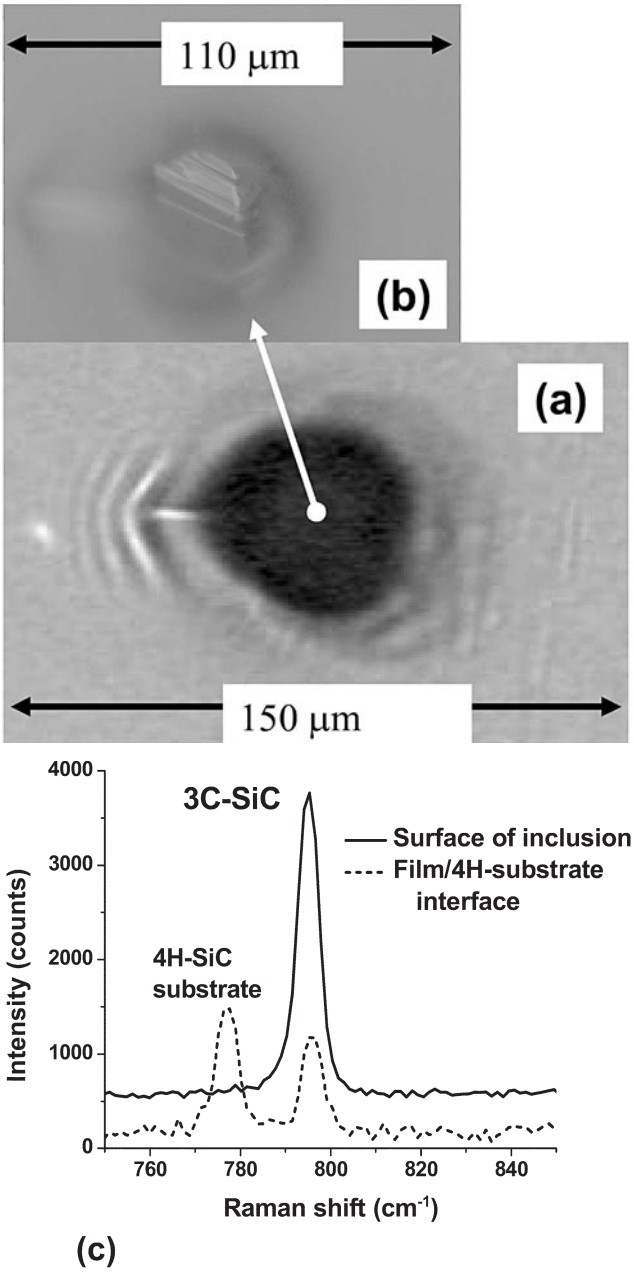

Fig. 6. (a) Microscope image of a large hole containing a core of crystalline SiC. (b) The core comes into focus 20 μm above the surface of the hole. (c) The Raman data shows that the core is 3C-SiC (solid line) and that it starts near the substrate/epilayer interface (dashed). The substrate is 4H-SiC.

focus 15 μm deeper into the hole. The area comprising the lip (dashed line) of the hole and areas around the hole are all unstrained 4H-SiC. The data suggest that this inclusion formed late in the growth process. From the ratio of intensities of the Raman modes of the 4H-SiC and the 6H-SiC, we estimate that the inclusion is approximately 1–2 μm in depth.

The final type of inclusion that we consider is one that is at the surface level but physically isolated from the surrounding material. Figure 8a shows an image of an inclusion that intersects the wafer surface and that is separated from the surrounding

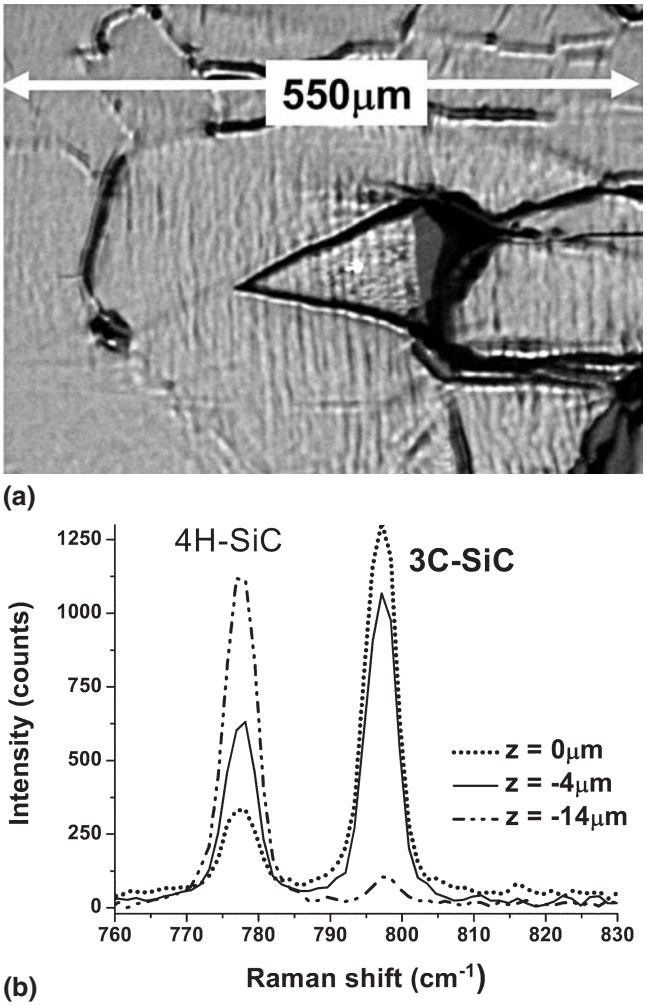

Fig. 7. (a) Microscope image of a smaller hole containing a core of crystalline SiC. The core comes into focus 5 μm below the surface of the hole. (b) The Raman data shows that the core consists of 6H-SiC (solid line) as well as 4H-SiC.

material by either cracks or grain boundaries. Note that it has a triangular shape and is about 150 μm in length. Interestingly, even though it is well separated from the surrounding material, its surface texture is similar to that of the material around it.

Figure 8b shows the Raman spectra taken from the triangular region. The region within the triangle is identified as mainly 3C-SiC with a small component of 4H-SiC (25% from peak intensities). As the focal point is moved down, the polytype changes from 3C-SiC to 4H-SiC. At a depth of 14 μm, the 3C-SiC Raman mode is no longer detected. From the peak intensities, we estimate that the 3C-SiC layer at the surface is approximately 10 μm in thickness. The region outside the triangle is unstrained 4H-SiC.

CONCLUSIONS

Cross-polarized imaging using an optical scanner has been used to reveal defects in n-4H-SiC. A new form of polarized imaging using a combination of linear and circular polarization has been reported.

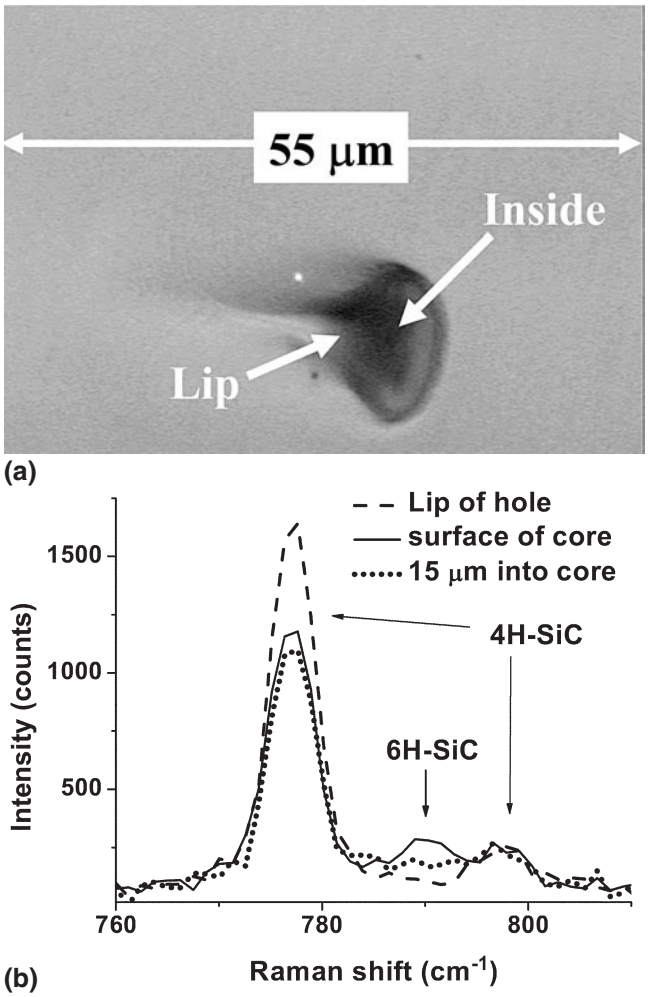

Fig. 8. (a) A microscope image of a large, isolated, triangular-shaped inclusion. The position of the Raman probe is shown as a small white circle near the center of the inclusion. (b) The Raman data is presented as a function of depth moving into the inclusion.

This mode improves contrast from defect-related features and reveals doping density variations.

Confocal μ-Raman spectroscopy has been used to investigate various features that are revealed by cross-polarized imaging. We have observed that regions of adjacent light and dark contrast can be two different types of defects: (a) regions with sharp lines of delineation are usually strained with bright contrast having a greater strain than sections with darker contrast and (b) regions with gradual contrast transitions tend to contain low-angle grain boundaries. We have observed that polytype inclusions can occur at any point in the growth. Two types of inclusions have been observed: those inside an empty cavity in the epitaxial layer and those that are part of flat regions that are outlined by cracks or grain boundaries. Both 3C-SiC and 6H-SiC inclusions have been observed. In all cases, the material containing the foreign polytype inclusion is strain free.

The combination of cross-polarized imaging and confocal μ-Raman spectroscopy is a powerful tool for defect detection and investigation in single-crystal bulk and epitaxial SiC. Confocal Raman spectroscopy not only allows us to identify the physical nature of a defect signature in polarized light imaging but also allows us to probe its physical extent with high spatial resolution. Further transmission-electron microscopy studies at areas of light contrast identified by cross-polarized imaging and μ-Raman spectroscopy would provide detailed identification of growth-related defects in SiC.

ACKNOWLEDGEMENTS

This work was supported in part by the Office of Naval Research and by the DARPA High Power Electronics Program.

REFERENCES

1. M. Bhatnagar and B.J. Baliga, *IEEE Trans. Electron Dev.* 40, 645 (1993).
2. T.P. Chow and M. Ghezzo, *Mater. Res. Soc. Symp. Proc.* 423, 9 (1996).
3. C.E. Weitzel and K.E. Moore, *Mater. Res. Soc. Symp. Proc.* 483, 111 (1998).
4. B.J. Baliga, *Mater. Res. Soc. Symp. Proc.* 512, 77 (1998).
5. C.H. Carter, Jr., R.P. Devaty, and G.S. Rohrer, eds., *Silicon Carbide and Related Materials 1999* (Lausanne, Switzerland: Trans Tech, 2000), pp. 469–472.
6. J.A. Cooper, Jr. and A. Agarwal, *Proc. IEEE* 90, 956 (2002).
7. J. Zhang, L. Storasta, J.P. Bergman, N.T. Son, and E. Janzen, *J. Appl. Phys.* 93, 4708 (2003).
8. A. Galeckas, V. Grivickas, J. Linnros, H. Bleichner, and C. Hallin, *J. Appl. Phys.* 81, 3522, (1997).
9. H. Lendenmann, F. Dahlquist, N. Johansson, R. Soderholm, P.A. Nilsson, J.P. Bergman, and P. Skytt, *Mater. Sci. Forum* 353, 727 (2000).
10. J.P. Bergman, H. Lendenmann, P.A. Nilsson, U. Lindenfelt, and P. Skytt, *Mater. Sci. Forum* 353, 299 (2000).
11. X. Ma, M. Parker, and T.S. Sudarshan, *Appl. Phys. Lett.* 80, 3298 (2002).
12. S. Milita, R. Madar, J. Baruchel, M. Anikin, and T. Argunova, *Mater. Sci. Eng. B* 61–62, 63 (1999).
13. M. Dudley and X.R. Huang, *Mater. Sci. Forum* 338–342, 431 (2000).
14. A. Haouni, M. Mermoux, B. Marcus, L. Abello, and G. Lucazeau, *Diamond Related Mater.* 8, 657 (1999).
15. D. Olego, M. Cardona, and P. Vogl, *Phys. Rev.* B25, 3878 (1982).
16. C. Hagiwara, K.M. Itoh, J. Muto, H. Nagasawa, K. Yagi, H. Harima, K. Mizoguchi, and S. Nakashima, *Mater. Sci. Forum* 264–268, 669 (1998).
17. S. Nakashima and H. Harima, *Phys. Status Solidi A* 162, 39 (1997).
18. L. Bergman, M. Dutta, C. Balkas, R.F. Davis, J.A. Christman, D. Alexson, and R.J. Nemanich, *J. Appl. Phys.* 85, 3535 (1999).